Micro and nano indentation studies on $Zr_{60}Cu_{10}Al_{15}Ni_{15}$ bulk metallic glass

S. Vincent[1], B. S. Murty[2], M. J. Kramer[3] and J. Bhatt[1*]

[1]Department of Metallurgical and Materials Engineering, V.N.I.T., Nagpur-440010, India

[2]Department of Metallurgical and Materials Engineering, Indian Institute of Technology Madras, Chennai-600036, India

[3]Ames Laboratory, U.S. Department of Energy, Iowa State University, Ames, Iowa-50011, U.S.A.

Abstract

Partially vitrified $Zr_{60}Cu_{10}Al_{15}Ni_{15}$ bulk metallic glass has been synthesized using water cooled copper mold drop casting technique. Kinetically favorable microstructures having different morphologies are observed throughout the volume of the bulk metallic glass sample. X-ray diffraction studies indicate formation of hard intermetallic compounds such as Zr_3Al_2 and Zr_2Ni in certain regions along with amorphous structures. Microindentation studies carried out in different regions of the sample reveal microstructure dependent deformation behavior. Highest hardness is observed in the fully crystallized regions compared to pure glassy regions in the same sample. Further nanoindenation in the same sample is used to understand dynamic mechanical properties of microstructures in different regions. The pile-up morphologies around the indent and differences in load-displacement curves provide vital information on deformation behavior of sample in different microstructure sensitive regions.

Keywords: Bulk metallic glass; Intermetallics.

*Corresponding author Tel: +91-712-2801513, Email: jatinbhatt@mme.vnit.ac.in (J. Bhatt)

1. Introduction

If high hardness and strength, excellent corrosion and wear resistance along with good castability and printability makes bulk metallic glasses (BMGs) superior than crystalline materials, their limited room temperature ductility acts as a barrier for structural applications [1]. This drawback leads to catastrophic failure arising due to highly localized shear band formation which is primary deformation mechanism in BMGs [2–4]. However, significant improvement in plasticity of BMGs has been reported by preparing BMG matrix composites (BMGMCs) [5–7]. The introduction of crystalline phases in BMG matrix promotes multiple shear band formation due to the existence of second phase, thus restricting shear localization and propagation of critical shear bands leading to pronounced plasticity in BMGMCs [5–7].

In recent years, micro and nano indentation techniques have emerged as significant tools to determine mechanical properties of BMGs. Quite a few reports are devoted to investigate underlying deformation mechanism of BMGs using indentation techniques [8–10]. Schuh and Nieh [11] have examined the mechanical properties of metallic glasses at the length scale of shear bands through nanoindentation. The study revealed serrated flow behavior of metallic glasses and the effect of indentation loading rates was addressed. Further, microstructural investigation of shear bands around the indented regions in BMGs was carried out to understand the nature of shear banding [12, 13]. Ramamurty and coworkers [14–16] have reported detailed analysis on plastic deformation through shear banding in various BMGs. However limited work has been carried out on indentation studies of BMGMCs [17, 18]. Further deformation studies on the same multicomponent system having different microstructural features are not reported to the best of author's knowledge and thus this provides motivation for the present work.

BMGMCs can be formed either by 'ex-situ' methods through addition of secondary phase particles or by 'in-situ' methods by controlling processing conditions [5–7]. Interestingly, lower cooling rate during solidification of liquid alloy melt also results in emergence of crystalline phases in a glassy matrix [19]. Insufficient cooling rate fails to suppress the nucleation and growth of crystalline phases during vitrification of alloy melt. On similar lines, in the present work $Zr_{60}Cu_{10}Al_{15}Ni_{15}$ BMG was prepared by drop casting method without any aid of suction, which has resulted in the coexistence of crystalline phases along with glassy phase. Three microstructurally distinct regions have been identified in the sample. Micro and nano indentations have been carried out in these regions of the sample to examine microstructure dependent deformation behavior. Further, indentation morphology analysis aims to provide significant information on deformation mechanism of the sample.

2. Experimental Details

Bulk metallic glass forming composition $Zr_{60}Cu_{10}Al_{15}Ni_{15}$ (at.%) was prepared by arc melting of pure elements (99.9% Zr and 99.99% Cu, Al and Ni) in a purified argon atmosphere. In order to achieve compositional homogeneity, the ingots were remelted several times. The alloy was then subjected to drop casting into water cooled copper mold without any aid of vacuum suction to obtain 6 mm diameter and 20 mm long BMG composite rod. The structure of rod at different regions was studied using X-ray diffraction (XRD) with Co-Kα radiation. The 6mm diameter cylindrical sample was vertically cut into two halves with one halve cold mounted in epoxy for microstructural examination. The mounted sample was polished using colloidal silica and etched with 45ml HNO_3, 10ml HF and 45ml H_2O.

Microhardness tests were conducted on the mounted, polished and etched sample using Mitutoyo Vickers microhardness testing machine. The tests were performed according to

ASTM: E-384 standards. The test were carried out at four different loads of 100, 200, 300 and 500g and average value of 8 indentations at each load with data scatter of ± 1% is reported. The indentation morphology after microhardness test was observed using JEOL JSM-6380A scanning electron microscope (SEM).

Nanoindentation experiments were conducted using TI 950 TriboIndenter with a Berkovich triangular diamond indenter. The indentations were performed in the load-control mode with a maximum load of 80 mN at a constant loading/unloading rate of 0.8mN/s. Ten indentations were performed to verify the accuracy and scatter of the indentation data. The impression of indent after complete unloading was examined using in-situ scanning probe microscopy (SPM) equipped with TriboIndenter.

3. Results and Discussion

3.1 XRD and Microindentation Studies

$Zr_{60}Cu_{10}Al_{15}Ni_{15}$ BMG prepared using drop casting has been characterized by XRD at different regions of the sample (Fig. 1). One end of the sample having the highest cooling rate has resulted in glassy phase and crystalline phases were observed at the other end owing to its lower cooling rate. In the intermediate region of the sample, a mixture of crystalline and glassy phases was observed. Thus, three distinct microstructurally different regions have been identified in the sample namely, region (A) representing complete amorphous phase, region (B) representing partially crystalline phase and region (C) representing complete crystalline phase. More detailed discussion on evolution of phases has been addressed elsewhere (yet to be published). A region transforming from amorphous to partially crystalline and finally to complete crystalline is identified in the sample (Fig. 1). Microindentation at 500 g load has been carried out at these regions.

Fig. 1 shows indentation morphology observed in SEM and corresponding XRD data at the 3 regions i.e., A, B and C. XRD of region (A) demonstrates broad diffraction hump and absence of any sharp crystalline peaks confirming its amorphous structure. Region (A) exhibits a hardness of 4.75±0.05 GPa at 500 g load as shown in Fig. 1. The indentation morphology at this region clearly reveals formation of large number of shear bands (shown by white arrow in Fig. 1). It is well known that glassy phase when subjected to indentation exhibits deformation with the aid of shear band formation which can be explained based on free volume concepts [13]. Due to large free volume in the glassy region, atoms move freely upon indentation and accumulate at certain regions, thus resulting in formation of shear bands. It is interesting to note that shear bands can be seen only at two adjacent sides of the indent (indicated by white arrow in Fig. 1). Shear bands were absent on the other two adjacent sides, towards partially crystalline region. This can be attributed to the presence of glass/crystal interface at the adjacent side which results in annihilation of free volume owing to dense packing of atoms. This further strengthens the free volume concept that as cluster of atoms move away from amorphous phase towards crystalline region, free volume reduces and thus atomic movement is restricted. Also, change in mode of plastic deformation is evident due to presence of crystalline phases.

XRD of partially crystalline phase at region (B) of the sample shows evolution of crystalline peaks. The crystalline peaks correspond to hard intermetallic Zr_3Al_2 (tetragonal) and Zr_2Ni (cubic) phases. Earlier, the formation of Zr_2Cu and Zr_3Al_2 intermetallic phases has been reported in Zr-Cu-Al-Ni BMG [20, 21]. In the present work, the evolution of Zr_2Ni phase has been reported instead of Zr_2Cu. This can be attributed to higher Ni content than Cu in the present composition $Zr_{60}Cu_{10}Al_{15}Ni_{15}$ in comparison to those reported in the literature

($Zr_{55}Cu_{30}Al_{10}Ni_5$,$Zr_{65}Cu_{17}Al_8Ni_{10}$) [20, 21]. The evolution of Zr_3Al_2 and Zr_2Ni intermetallic phases from Zr-Cu-Al-Ni alloy can also be explained on the basis of chemical interaction among different elements. Binary enthalpy of mixing values [22] ($\Delta H_{Zr\ in\ Ni} = -236$,$\Delta H_{Zr\ in\ Al} = -189$, $\Delta H_{Zr\ in\ Cu} = -110$, $\Delta H_{Al\ in\ Ni} = -96$, $\Delta H_{Al\ in\ Cu} = -34$, $\Delta H_{Cu\ in\ Ni} = +14$) calculated from Gallego's approach [23] indicates that Zr_3Al_2 and Zr_2Ni phases, having the highest negative enthalpy of mixing of –41.76 and –41.66 kJ/mol, respectively, are the most stable phases to form in Zr-Cu-Al-Ni system.

Broad amorphous hump can be observed below the crystalline peaks at region (B) in the Fig. 1 indicating that cooling rate in this region is such that crystallization of the liquid is not complete and some residual liquid has undergone vitrification. Microhardness at 500 g load indicates a hardness value of 5.30±0.05 GPa at this region. Hardness at region (B) is found to be higher than that of amorphous region (A) owing to the presence of hard intermetallic phases. SEM analysis of indentation morphology at region (B) (Fig. 1) does not show any shear bands. This can be attributed to decrease in free volume due to structural relaxation of the glass by formation of closely packed atomic configuration. The amorphous hump indicated by XRD is due to residual glassy phase. The presence of crystalline phases i.e. Zr_3Al_2 and Zr_2Ni act as obstacles restricting atomic mobility thereby increasing resistance to plastic deformation by arresting shear band propagation. This could be the possible reason for increase in hardness and absence of shear bands in this region.

XRD pattern of region (C) in Fig. 1 shows complete crystallization. Crystalline phases Zr_3Al_2 and Zr_2Ni are more prominent in this region in comparison with region (B). Microhardness of region (C) indicates the highest hardness in comparison with region (A) and (B). Hardness value of 5.70±0.05 GPa is observed (shown in Fig. 1) at a load of 500 g. The highest hardness

in this region can be attributed to the complete crystallization of the liquid to hard intermetallic Zr_3Al_2 and Zr_2Ni crystalline phases. SEM analysis of indentation morphology at region (C) (Fig. 1) does not reveal shear bands. Complete crystallization leads to strong interatomic bonds due to formation of intermetallic phases and thus resistance to atomic mobility further increases. As a result, highest hardness is reported in this region.

The microhardness of the sample at 3 different regions using 100, 200, 300 and 500 g loads are shown in Fig. 2. The highest hardness is observed in fully crystalline region followed by partially crystalline region. Amorphous region is reported to show the lowest hardness. Interestingly, earlier investigations have revealed the highest hardness in super cooled liquid state in comparison with crystallized state [24, 25]. It has been pointed out that due to structural relaxation in this state, annihilation of free volume takes place leading to restricted shear band movement and thus increase in hardness. A few studies indicating the highest hardness in the partially crystallized state have also been reported [13, 26]. This has been attributed to presence of nanocrystals which suppress shear band multiplication and therefore increase in hardness. However, complete crystallization of glassy matrix in the earlier studies has resulted in decrease in hardness, reasons pointed out being the weak intercrystalline interfaces and increase in defects [13].

In the present investigation, the highest hardness in the complete crystallization region is attributed to formation of stable intermetallic phases. As discussed above, Zr_3Al_2 and Zr_2Ni are both thermodynamically stable phases which results in strong intercrystalline interface. Zr_3Al_2 with tetragonal primitive (tP) structure has the lattice parameters of a = 7.630 nm and c = 6.998 nm [27]. Zr_2Ni with cubic face centered (cF) structure has a lattice parameter of a = 12.27 nm [28]. The significant differences between two phase lattice results in incoherent

interface due to large lattice misfit. Such sufficiently large atomic misfit at the interface results in dislocation pile ups leading to increase in strain which further strengthens the crystalline interface. Thus it results in additional strengthening against moving dislocations and further increase in hardness [29]. Wang *et al.* [20] have also reported increase in hardness with the formation of Zr_3Al_2 and Zr_2Cu phases in Zr-Cu-Al-Ni system which further strengthens the present argument. It is important to note that hardness can also be composition specific in BMGs.

3.2 Nanoindentation Studies

Load (P) – displacement (h) curve obtained by nanoindentation on each of the 3 different regions i.e. amorphous, partially crystalline and crystalline regions are presented in Fig. 3 (a). The hardness (H) and elastic modulus (E) obtained from curve using Oliver-Pharr method [30] are shown in Table 1. They show the following trend.

$$H_c > H_{p\text{-}c} > H_a \quad (1)$$

$$E_c > E_{p\text{-}c} > E_a \quad (2)$$

where ‘c’, ‘p-c’ and ‘a’ represents crystalline, partially crystalline and amorphous region, respectively. Hard intermetallic crystalline phases i.e. Zr_3Al_2 and Zr_2Ni exhibit the highest hardness and elastic modulus of 8.33 and 131.3 GPa, respectively. H/E ratio [9] which indicates elastic recovery of material is > 0.05 (Table 1) for all 3 regions. However, crystalline region demonstrates the highest H/E ratio suggesting a high degree of elastic recovery in comparison with amorphous and partially crystalline regions. Since the hardness and elastic modulus increase proportionally in the amorphous and partially crystalline regions, they indicate similar H/E ratios. The present results are in agreement with the previous ones [31] which suggest H/E ratios for BMGs to be in range of 0.05~0.06.

It is evident that hardness values obtained by the nanoindentation are higher in comparison with the microindentation results. This phenomenon is often referred as indentation size effect (ISE) [32, 33]. A model based on dislocations has been proposed to explain ISE [34]. During small indentations (lower loads), shear field created by the indenter results in distorted crystal lattice. Thus, geometrically necessary dislocations have to be created in order to form the residual indentation imprints. In case of large indentations, the strain variations between two extremes are more gradual. As a result, shear stress can easily be accommodated in statistically stored dislocations without the need of geometrically necessary dislocations. Hence nanoindentation exhibits higher hardness than microindentation. This explanation holds good for crystalline materials. BMGs lack defects such as dislocations, yet they exhibit ISE. Jang *et al.* have proposed a model to explain ISE in BMGs [35]. BMGs are reported to exhibit strain softening during plastic deformation rather than strain hardening due to shear localization. As a result, local rearrangement of atoms takes place to accommodate shear strain leading to shear transformation zones (STZs) [36]. During small indentations, the shear field is too small to have sufficient population of STZs and thus shear bands are forced to operate at particular locations leading to increase in hardness. In case of higher loads, large volume of deformation leads to higher activities of STZs and shear bands and thus results in decrease in hardness.

The reports on ISE so far are on either separate crystalline materials or amorphous materials. This study presents unique case in which ISE is observed in both glassy region as well as crystalline region in single multicomponent system. This further clarifies that ISE is a global phenomenon and not restricted to crystalline materials. The ISE phenomenon is also observed in microindentation result (Fig. 2) in which there is decrease in hardness with increase in load. Apart from this, variation in hardness with respect to change in microstructure is also

observed. The above discussion based on creation of geometrically necessary dislocations and lack of STZ populations for smaller load can be reason for ISE during microindentation. Also, the formation of thermodynamically stable intermetallic phases and annihilation of free volume could be possible reasons for variation in hardness with respect to microstructural features. Both, micro and nanoindentations follow same trend which demonstrate highest hardness in completely crystallized region followed by partially crystallized region and amorphous region.

The magnified P-h curves in Fig. 3(b) demonstrate highly serrated flow in the amorphous region (indicated by arrow). Few serrations were also observed in P-h curve of partially crystalline and fully crystalline region. Schuh and Nieh [11] has carried out extensive analysis on plastic flow behavior of BMGs and reported that serrations in glassy alloys mainly depend on loading rate employed. It has been suggested that smaller loading rates (0.04 mN/s) promote more prominent serrations in contrast to higher loading rates (5 mN/s) which suppress serrated flow. In the present investigation, intermediate loading rate (0.8 mN/s) also exhibits high rate of serrated flow as shown by arrows in Fig. 3(b). The distance between each serrations is around 8 – 10 nm wide in the amorphous region.

The serrations in the P-h curve are termed as ‘pop-in’ event. It has been suggested that these discrete ‘pop-in’ events corresponds to nucleation and propagation of individual shear bands [11, 37]. This further suggests that large numbers of shear bands are activated during indentation in the amorphous region. The morphology of surface after nanoindentation for amorphous, partially crystalline and crystalline regions is presented in Fig. 4 (a) – (c). Quite a few prominent shear bands can be seen in Fig. 4(a) which is evident as large number of ‘pop-in’ events in P-h curve of amorphous region. Although a few serrations are observed in P-h

curve of partially and fully crystalline regions (Fig. 3(b)), the indentation morphology does not reveal any shear band formation in partially crystalline (Fig. 4 (b)) and crystalline regions (Fig. 4 (c)). This can be attributed to the fact that all the 'pop-in' events cannot be accounted for shear bands since pop-ins can lead to nucleation and propagation of shear bands inside of the material as well. The serrations observed in partially and fully crystalline regions could be due to following reasons. During indentation, there could be local rise in temperature in regions in close proximity at indent-material interface. This rise in temperature may suffice the energy required to localized melting. This being dynamical change which is followed by continuous loading of indenter that may cover up local atomic environments and result into pop-in events giving serrations patterns in P-h curve for amorphous phase. Such hypothesis requires further investigation to understand mechanism on change in local environments upon dynamic loading on structurally sensitive muticomponent amorphous materials.

4. Conclusions

Systematic study of micro and nano indentations on different regions of $Zr_{60}Cu_{10}Al_{15}Ni_{15}$ BMG has been carried out. Fully crystalline region exhibits the highest hardness in comparison with partially crystalline and glassy regions and the possible reasons are (i) the formation of thermodynamically stable intermetallic phases i.e. Zr_3Al_2 and Zr_2Ni resulting in strong intercrystalline interface (ii) due to large lattice misfit between two different phases provides additional hardening against moving dislocations. Further, this study presents a unique case in which ISE is observed in glassy as well as crystalline regions in single multicomponent systems. Indentation morphology analysis further strengthens the micro and nanoindentation results in which clear shear band propagation is observed in amorphous region owing to presence of free volume.

Acknowledgement

One of the Author's, Jatin Bhatt, is thankful to INDO US Science and Technology forum for Fellowship award (IUSSTF Fellowship/16-2012) to carry out part of above research work at Ames Laboratory (US-DOE), Iowa State University, USA. This work was supported by the U.S. Department of Energy (DOE), Office of Basic Energy Science, Division of Materials Science and Engineering. The research was performed at the Ames Laboratory, which is operated for the U.S. DOE by Iowa State University under contract DE-AC02-07CH11358. The authors' are also thankful to Technical Education Quality Improvement Program (TEQIP II), Government of India for providing financial assistance.

References

1. Wang WH, Dong C, Shek CH. Bulk metallic glasses. Mater. Sci. Eng. R 2004; 44:45–89.
2. Zhang ZF, He G, Eckert J, Schultz L. Fracture mechanisms in bulk metallic glassy materials. Phys. Rev. Lett. 2003; 91:45505.
3. Flores KM, Dauskart RH. Mean stress effects on flow localization and failure in a bulk metallic glass. Acta Mater. 2001; 49:2527–37.
4. Conner RD, Dandliker RB, Johnson WL. Mechanical properties of tungsten and steel fiber reinforced $Zr_{41.25}Ti_{13.75}Cu_{12.5}Ni_{10}Be_{22.5}$ metallic glass matrix composites. Acta Mater. 1998; 46:6089–102.
5. Liu YH, Wang G, Wang RJ, Zhao DQ, Pan MX, Wang WH. Superplastic bulk metallic glasses at room temperature. Science 2007; 315:1385–8.
6. Qiu F, Shen P, Liu T, Jiang Q. Enhanced ductility in a $Zr_{65}Cu_{15}Al_{10}Ni_{10}$ bulk metallic glass by nanocrystallization during compression. Mater Des. 2012; 36:168–71.

7. Qiao JW, Zhang Y, Chen GL. Fabrication and mechanical characterization of a series of plastic Zr-based bulk metallic glass matrix composites. Mater Des. 2009; 30:3966–71.
8. Mukhopadhyay NK, Paufler P. Micro- and nanoindentation techniques for mechanical characterisation of materials. Int. Mater. Rev. 2006; 51:209–45.
9. Mukhopadhyay NK, Belger A, Paufler P, Kim DH. Nanoindentation studies on Cu–Ti–Zr–Ni–Si–Sn bulk metallic glasses. Mater. Sci. Eng. A 2007; 449–451:954–7.
10. Bhatt J, Pabi SK, Murty BS. Nanoindentation studies on amorphous, Nanoquasicrystalline and nanocrystalline $Zr_{80}Pt_{20}$ and $Zr_{75}Pd_{25}$ alloys. J. Nanosci. Nanotechnol. 2007; 7:658–62.
11. Schuh CA, Nieh TG. A nanoindentation study of serrated flow in bulk metallic glasses. Acta Mater. 2003; 51:87–99.
12. Vaidyanathan R, Dao M, Ravichandran G, Suresh S. Study of mechanical deformation in bulk metallic glass through instrumented indentation. Acta Mater. 2001; 49:3781–89.
13. Vincent S, Basu J, Murty BS, Bhatt J. Micro indentation study on $Cu_{60}Zr_{20}Ti_{20}$ metallic glass. Mater. Sci. Eng. A 2012; 550:160–6.
14. Ramamurty U, Jana S, Kawamura Y, Chattopadhyay K. Hardness and plastic deformation in a bulk metallic glass. Acta Mater. 2005; 53:705–17.
15. Jana S, Ramamurty U, Chattopadhyay K, Kawamura Y. Subsurface deformation during Vickers indentation of bulk metallic glasses. Mater Sci Eng A 2004; 375–377:1191–5.
16. Jana S, Bhowmick R, Kawamura Y, Chattopadhyay K, Ramamurty U. Deformation morphology underneath the Vickers indent in a Zr-based bulk metallic glass. Intermetallics 2004; 12:1097–102.
17. Raghavan R, Shastry VV, Kumar A, Jayakumar T, Ramamurty U. Toughness of as-cast and partially crystallized composites of a bulk metallic glass. Intermetallics 2009; 17:835–9.

18. Narayan RL, Boopathy K, Sen I, Hofmann DC, Ramamurty U. On the hardness and elastic modulus of bulk metallic glass matrix composites. Scripta Mater. 2010; 63:768–71.
19. Perepezko JH, Santhaweesuk C, Wang JQ, Imhoff SD. Kinetic competition during glass formation. J. Alloys Comp. 2013; DOI: 10.1016/j.jallcom.2013.11.220.
20. Wang CS, Chi LN, Dong C. Influence of (Zr,C) content on microstructure and properties of $Zr_{55}Al_{10}Ni_5Cu_{30}$ alloy prepared by laser-induced self-propagating reaction synthesis. Mater. Sci. Eng. A 2007; 449–451:609–12.
21. Wang XD, Yi S. Effect of Zr/Ni ratio on the stability and ductility of Zr–Al–Ni–Cu bulk metallic glasses. Mater. Sci. Eng. A 2007; 449–451:613–6.
22. Niessen AK, deBoer FR, Boom R, deChatel PF, Mattens WCM, Miedema AR. Model predictions for the enthalpy of formation of transition metal alloys II. Calphad 1983; 7:51–70.
23. Gallego LJ, Somoza JA, Alonso JA. Glass formation in ternary transition metal alloys. J. Phys. Condens. Matter 1990; 2:6245–50.
24. Concustell A, Alcalá G, Mato S, Woodcock TG, Gebert A, Eckert J, Baró MD. Effect of relaxation and primary nanocrystallization on the mechanical properties of $Cu_{60}Zr_{22}Ti_{18}$ bulk metallic glass. Intermetallics 2005; 13:1214–9.
25. Bhatt J, Kumar S, Dong C, Murty BS. Tribological behaviour of $Cu_{60}Zr_{30}Ti_{10}$ bulk metallic glass. Mater. Sci. Eng. A 2007; 458:290–4.
26. Kim YH, Higara K, Inoue A, Masumoto T, Jo HH. Crystallization and high mechanical strength of Al based amorphous alloys. Mater. Trans. JIM 1994; 35:293–302.
27. Wilson CG, Spooner FJ. The crystal structure of $ZrAl_2$. Acta Crystallogr. 1960; 13:358–9.

28. Altounian Z, Batalla E, Strom-Olsen JO, Walter JL. The influence of oxygen and other impurities on the crystallization of $NiZr_2$ and related metallic glasses. J. Appl. Phys. 1987; 61:149–55.
29. Kawahara K, Kaneno Y, Kakitsuji A, Takasugi T. Microstructural factors affecting hardness property of dual two-phase intermetallic alloys based on Ni_3Al–Ni_3V pseudo-binary alloy system. Intermetallics 2009; 17:938–44.
30. Oliver WC, Pharr GM. An improved technique for determining hardness and elastic modulus using load and displacement sensing indentation experiments. J. Mater. Res. 1992; 7:1564–83.
31. Ohtsuki M, Nagata K, Tamura R, Takeuchi S. Tungsten-Based Metallic Glasses with High Crystallization Temperature, High Modulus and High Hardness. Mater. Trans. JIM 2005; 46:48–53.
32. Manika I, Maniks J. Size effects in micro- and nanoscale indentation. Acta Mater. 2006; 54:2049–56.
33. Steenberge NV, Sort J, Concustell A, Das J, Scudino S, Surinach S, Eckert J, Baro MD. Dynamic softening and indentation size effect in a Zr-based bulk glass-forming alloy. Scripta Mater. 2007; 56:605–8.
34. Nix WD, Gao H. Indentation size effects in crystalline materials: A law for strain gradient plasticity. J. Mech. Phys. Solids 1998; 46:411–25.
35. Jang JI, Yoo BG, Kim YJ, Oh JH, Choi IC, Bei H. Indentation size effect in bulk metallic glass. Scripta Mater. 2011; 64:753–6.
36. Schuh CA, Hufnagel TC, Ramamurty U. Mechanical behavior of amorphous alloys. Acta Mater. 2007; 55:4067–109.
37. Golovin YI, Ivolgin VI, Khonik VA, Kitagawa K, Tyurin AI. Serrated plastic flow during nanoindentation of a bulk metallic glass. Scripta Mater. 2001; 45:947–52.

Figure captions

Figure 1: XRD and SEM indentation morphologies (load 500g) of $Zr_{60}Cu_{10}Al_{15}Ni_{15}$ BMG at different regions namely (A) amorphous region (B) partially crystalline region and (c) crystalline region. XRD pattern reveals evolution of Zr_3Al_2 and Zr_2Ni crystalline phases while SEM at amorphous region shows distinct shear bands formation.

Figure 2: Variation of hardness versus load at different regions of $Zr_{60}Cu_{10}Al_{15}Ni_{15}$ BMG.

Figure 3: (a) Load versus displacement at different regions of $Zr_{60}Cu_{10}Al_{15}Ni_{15}$ BMG and (b) magnified figure showing small 'pop-in' events in amorphous region of sample.

Figure 4: Nanoindentation morphology observed by in-situ SPM at (a) amorphous (b) partially crystalline and (c) crystalline regions. Distinct shear band can clearly be observed in the amorphous region of the sample

Table 1: Hardness (H), Elastic Modulus (E) and H/E ratios of $Zr_{60}Cu_{10}Al_{15}Ni_{15}$ BMG at amorphous, partially crystalline and crystalline regions.

Region	Hardness, H (GPa)	Elastic Modulus, E (GPa)	H/E ratio
Amorphous	5.95	111.2	0.053
Partially Crystalline	6.80	124.6	0.054
Crystalline	8.33	131.3	0.063

Vincent *et al*.

Figure 1

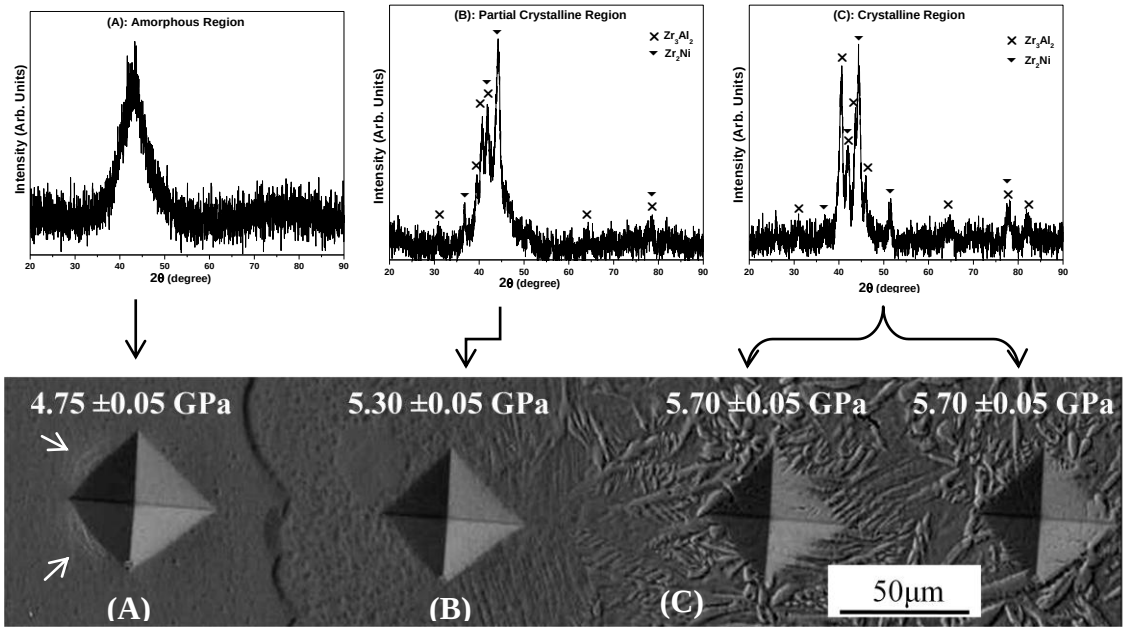

Figure 2

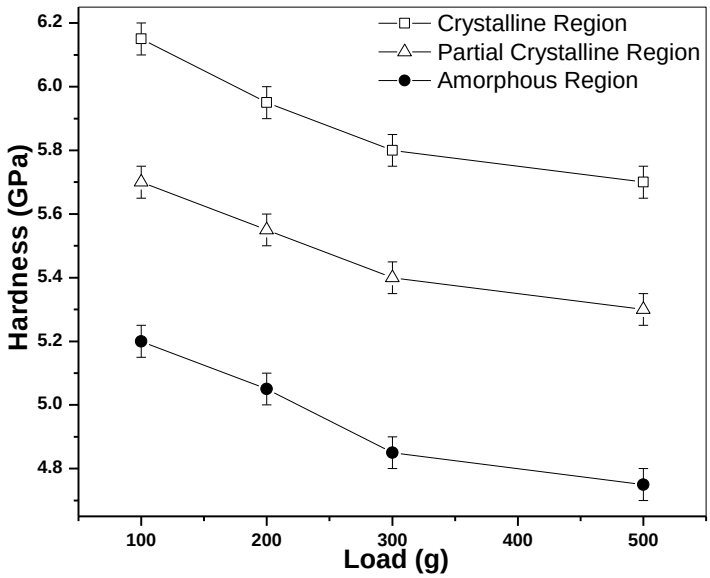
Crystalline Region
Partial Crystalline Region
Amorphous Region
Hardness (GPa)
6.2
6.0
5.8
5.6
5.4
5.2
5.0
4.8
100
200
300
400
500
Load (g)

Figure 3

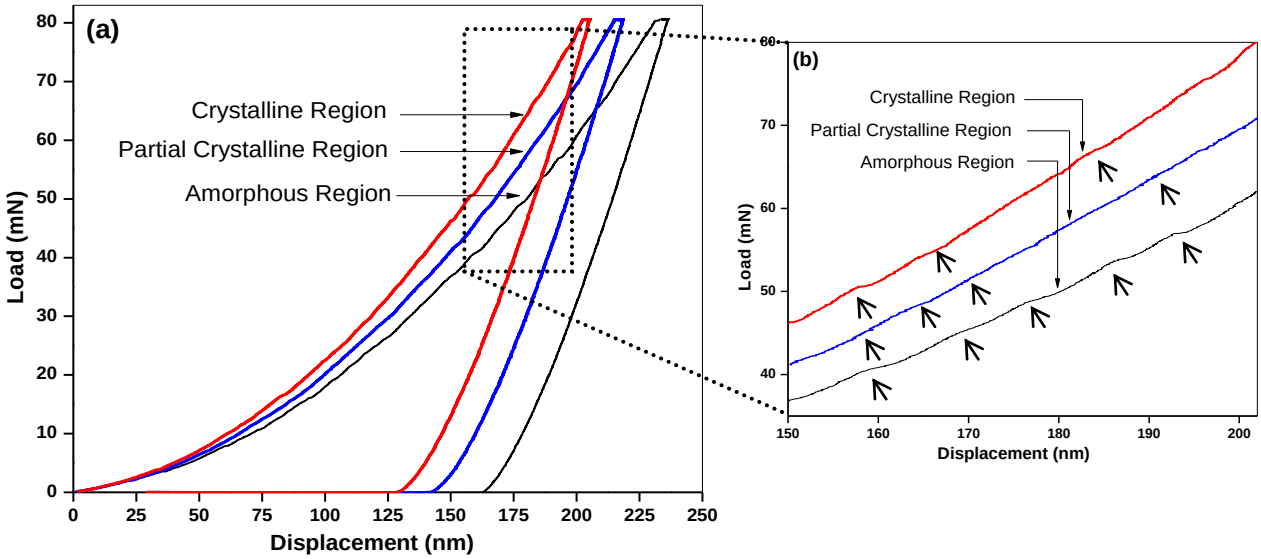
(a)
Crystalline Region
Partial Crystalline Region
Amorphous Region
Load (mN)
Displacement (nm)
(b)
Crystalline Region
Partial Crystalline Region
Amorphous Region
Load (mN)
Displacement (nm)

Vincent *et al*.

Figure 4